0026-895X/08/7401-264–273$20.00
MOLECULAR PHARMACOLOGY
Vol. 74, No. 1
41871/3353818
*Mol Pharmacol* 74:264–273, 2008
*Printed in U.S.A.*


# Characterization of mENT1Δ11, a Novel Alternative Splice Variant of the Mouse Equilibrative Nucleoside Transporter 1

Kevin R. Robillard,[1] Derek B. J. Bone, Jamie S. Park, and James R. Hammond

*Department of Physiology and Pharmacology, Schulich School of Medicine and Dentistry, University of Western Ontario, London, Ontario, Canada*

Received September 14, 2007; accepted April 14, 2008

**ABSTRACT**

Mammalian cells require specific transport mechanisms for the cellular uptake and release of endogenous nucleosides such as adenosine, and nucleoside analogs used in chemotherapy. We have identified a novel splice variant of the mouse equilibrative nucleoside transporter, mENT1, that results from the exclusion of exon 11 during pre-RNA processing. This variant encodes a truncated protein (mENT1Δ11) missing the last three transmembrane domains of the full-length mENT1. The mENT1Δ11 transcript and protein were found to be differentially distributed among tissues relative to full-length mENT1. PK15-NTD (nucleoside transport deficient) cells were transfected with mENT1 or mENT1Δ11 and assessed for nucleoside transport function. No significant differences were observed between the mENT1 and mENT1Δ11 in terms of transport function or inhibitor binding affinity. PK15-mENT1Δ11 transfected cells bound the ENT1 probe [$^3$H]nitrobenzylthioinosine (NBMPR) with high affinity and mediated the cellular accumulation of both [$^3$H]2-chloroadenosine and [$^3$H]uridine. The only significant differences between the mENT1 variants were that mENT1Δ11 could not be photolabeled with [$^3$H]NBMPR and that mENT1Δ11 was insensitive to the transporter-modifying effects of *N*-ethylmaleimide. These data suggest that the last three transmembrane domains of mENT1 are not necessary for transport activity, but this region does contain the cysteines responsible for the sensitivity of mENT1 to sulfhydryl reagents, and the residues important for covalent modification of the protein with NBMPR. These results provide important guidelines for future mutagenesis studies aimed at elucidating the tertiary structure of the ENT1 protein and the domains involved in inhibitor binding and substrate translocation.

Nucleosides and their therapeutic analogs are hydrophilic molecules that require a system to transport them from the extracellular environment into the cytoplasm of mammalian cells (Baldwin et al., 2004; King et al., 2006; Zhang et al., 2007). In most cell types, this occurs by facilitative diffusion through a family of equilibrative nucleoside transporters (ENTs) (Hyde et al., 2001). The best characterized of this family is ENT1, which is distinguished functionally by its high affinity for the inhibitor nitrobenzylmercaptopurine riboside (NBMPR; nitrobenzylthioinosine) (Hyde et al., 2001). ENT1 mediates the bidirectional transport of a variety of purine and pyrimidine nucleosides, including adenosine, which is known to have endogenous cardiovascular and neural regulatory functions. The *ENT1* gene was identified in human and rat tissues in 1997 (Coe et al., 1997; Griffiths et al., 1997; Yao et al., 1997), and we obtained the cDNA for the mouse ENT1 in 2000 (Kiss et al., 2000). The protein encoded by mENT1 is predicted to consist of 458 amino acids in an 11-transmembrane domain (TM) topology with a large glycosylated extracellular loop joining TMs 1 and 2, and a large intracellular loop between TMs 6 and 7 (Fig. 1). The central intracellular loop is predicted to contain phosphorylation sites for casein kinase II (CK2) and protein kinase C. We, and others, have identified an alternative splice variant of mENT1 that is missing a Lys-Gly in the central intracellular loop and has an arginine in place of a serine in the position (254) preceding the deletion (mENT1a; mENT1.2) (Kiss et

This study was supported by a Discovery Grant from the Natural Sciences and Engineering Research Council of Canada (to J.R.H.). K.R. gratefully acknowledges the financial support provided by the Schulich School of Medicine and Dentistry, University of Western Ontario, during the course of his graduate studies. D.B.J.B. is the recipient of an Ontario Graduate Scholarship in Science and Technology.

A preliminary report of this work was presented at the XVth World Congress of Pharmacology; 2006 July 2–7; Beijing, China.

[1] Current affiliation: Department of Pharmaceutical Sciences, Faculty of Pharmacy, University of Toronto, Toronto, Ontario, Canada.

Article, publication date, and citation information can be found at http://molpharm.aspetjournals.org.

doi:10.1124/mol.107.041871.

**ABBREVIATIONS:** ENT, equilibrative nucleoside transporter; NBMPR, nitrobenzylmercaptopurine riboside; TM, transmembrane; CK2, casein kinase II; bp, base pair(s); RT, reverse transcription; PCR, polymerase chain reaction; PBS, phosphate-buffered saline; NEM, *N*-ethylmaleimide; NBTGR, nitrobenzylthioguanosine riboside; CMV, cytomegalovirus; BGS, bovine growth serum; PVDF, polyvinylidene difluoride; TBS-T, Tris-buffered saline/Tween 20; NMG, *N*-methyl-glucamine; PAGE, polyacrylamide gel electrophoresis; PK15-NTD, pig kidney epithelial cells 15–nucleoside transport deficient; U2-OS, U2-osteosarcoma.

al., 2000; Handa et al., 2001). This results in the loss of a potential CK2 phosphorylation site. We have shown that this shorter variant differs from the full-length mENT1 in that it is insensitive to the transporter-modifying effects of CK2 inhibitors and has a significantly higher affinity for [$^3$H]N-BMPR (Bone et al., 2007).

We have now identified a third mENT1 variant that arises from the skipping of exon 11 during preRNA processing, designated mENT1Δ11 (GenBank accession no. EU180577). This variant was first noted as a 1242-bp RT-PCR product from mouse skeletal muscle when using primers to the open reading frame of mENT1 (1500 bp; GenBank accession no. AF131212.1). In silica translation of the sequence indicated that the protein encoded by this mRNA would be lacking 102 amino acids from the C terminus as a result of the introduction of a frame-shift resulting in a stop codon after position 356. Preliminary studies, presented at the XVth World Congress of Pharmacology (Robillard et al., 2006), showed that mENT1Δ11 encoded a protein that retained high affinity for [$^3$H]NBMPR. The present study reports on the complete characterization of this novel splice variant.

## Materials and Methods

**Materials.** Culture flasks were purchased from BD Biosciences (Franklin Lakes, New Jersey). Modified Eagle's medium, sodium pyruvate, nonessential amino acids, G418 (Geneticin), Lipofectamine 2000, penicillin/streptomycin solution, trypsin/EDTA solution, and culture-grade phosphate-buffered saline (PBS) were purchased from Invitrogen (Burlington, ON, Canada). *N*-Ethylmaleimide (NEM), 2-chloroadenosine, dipyridamole [2,6-bis(diethanolamino)-4,8-dipiperidino-pyridmido-[4,5-*d*]pyrimidine], NBMPR, nitrobenzylthioguanosine riboside [NBTGR; *S*-(4-nitrobenzyl)-6-thioguanosine], rabbit polyclonal anti-FLAG antibody, goat anti-rabbit antibody conjugated to horseradish peroxidase, p3×FLAG-CMV10 vector, protease inhibitor cocktail [4-(2-aminoethyl)benzenesulfonyl fluoride, pepstatin A, L-*trans*-epoxysuccinyl-leucylamido(4-guanidino)butane, bestatin, leupeptin, and aprotinin], and mRNA purification kits were purchased from Sigma-Aldrich (Oakville, ON, Canada. The anti-ENT1 antibody [ENT1 (K-15); affinity-purified polyclonal], raised to the C-terminal end of the central intracellular loop of ENT1 (amino acids 250–300), was from Santa Cruz Biotechnology (Santa Cruz, CA). Draflazine [2-(aminocarbonyl)-4-amino-2,6-dichlorophenyl)-4-[5,5-bis(4-fluorophenyl)pentyl]-1-piperazine acetamide 2HCl] was acquired from Janssen Research Foundation (Beerse, Belgium). Dilazep (*N*,*N*′-bis[3-(3,4,5-trimeth-oxybenzo-yloxy)propyl]-homo-piperazine) was provided by Asta Werke (Frankfurt, Germany). [$^3$H]NBMPR (5.5–20.1 Ci/mmol), [$^3$H]2-chloroadenosine (9.1 Ci/mmol), and $^3$H-labeled water (1 mCi/g) were purchased from Moravek Biochemicals (Brea, California). Oligonucleotide primers were purchased from Sigma-Genosys (Oakville, ON, Canada), and all restriction enzymes were from Fermentas International Inc. (Burlington, ON, Canada). Platinum Taq polymerase, Superscript First-Strand Synthesis System for RT-PCR, Pure-link Gel-Extraction Kit, DH5α *Escherichia coli,* the Benchmark Prestained Protein Ladder, and the pcDNA3.1TOPO kit were purchased from Invitrogen (Burlington, ON, Canada). Mini-prep Plasmid DNA kits were obtained from QIAGEN (Mississauga, ON, Canada), and cloning rings were purchased from Bel-Art Scienceware (Pequannock, New Jersey, USA). U2-osteosarcoma (U2-OS) cells were a gift from Dr David Litchfield (University of Western Ontario, London, ON, Canada) and the PK15-NTD (nucleoside transport deficient) cells used for creating the stable mENT1 cell lines were provided by Dr. Ming Tse (Johns Hopkins University, Baltimore, MD).

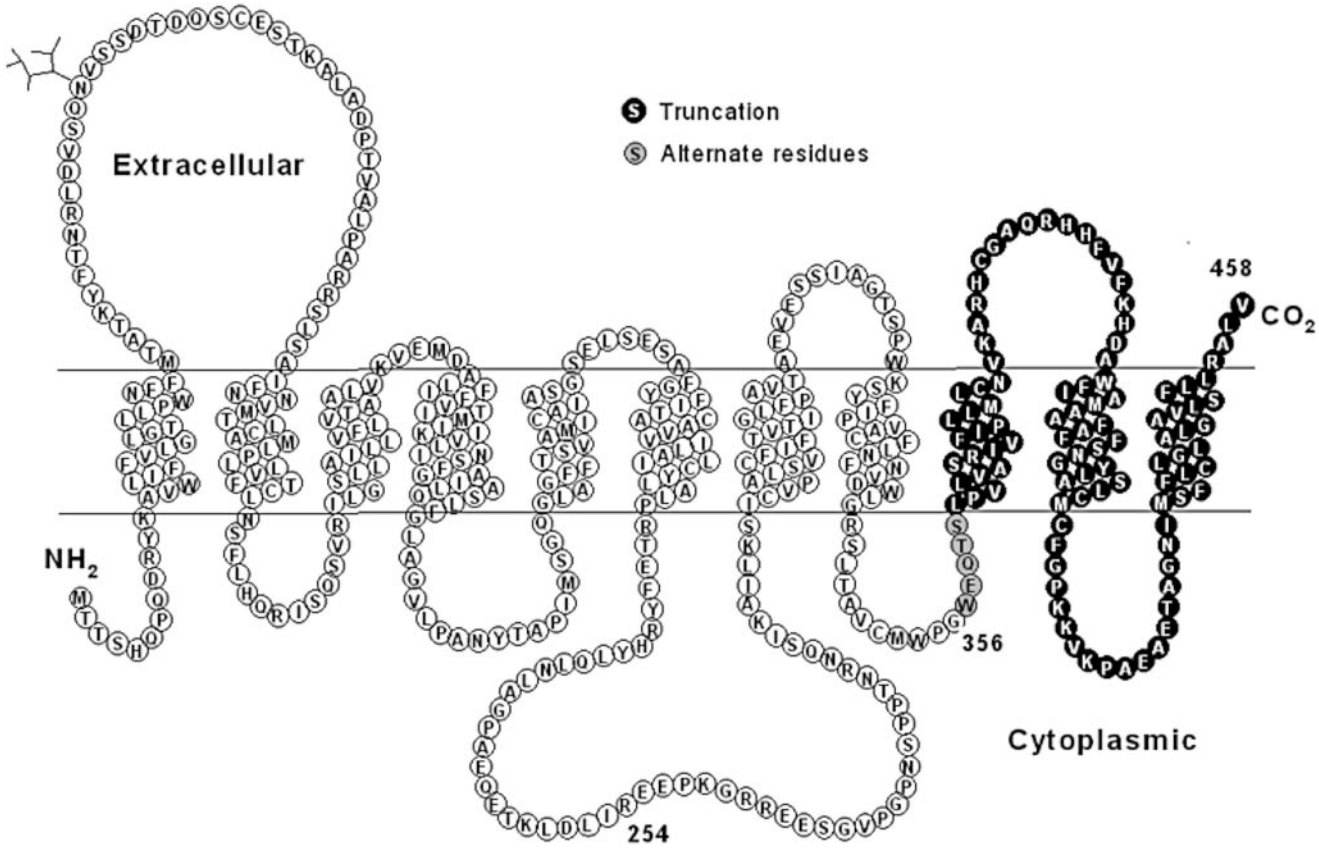


**Fig. 1.** Predicted topology of mENT1Δ11. The sequence is identical to mENT1 from the N-terminal to Gly356. Residues 357–361 are unique to mENT1Δ11, and residues 362–458 of mENT1 are missing from mENT1Δ11.

**Plasmid Generation.** mENT1 and mENT1Δ11 were obtained from mouse skeletal muscle tissue by RT-PCR using Platinum Taq polymerase and primers complementary to the 5′ and 3′ termini of the open reading frame of mENT1 (5′mENT1, 3′mENT1-Kpn1; Table 1). PCR conditions were as follows: initial activation for 5 min at 95°C, followed by 35 cycles of 30 s at 95°C, 30 s at 55°C, and 30 s at 72°C, and a final 10-min elongation at 72°C. The PCR products were ligated into the multiple cloning site of pcDNA3.1 using the TOPO cloning procedure. All constructs were sequenced in both directions (Robarts Research Institute, Sequencing Facility, London, ON, Canada) using the Taq BigDye Terminator Cycle Sequencing kit in an automated ABI PRISM model 377 Version 3.3 DNA sequencer (Applied Biosystems, Streetsville, ON, Canada). The nucleotide sequences were translated and transmembrane topology predictions were made using the Tmpred software (http://www.ch.embnet.org/software/TMPRED_form.html).

To generate plasmids encoding mENT1 or mENT1Δ11 with an N-terminal FLAG epitope tag (DYKYYYD), pcDNA3.1-mENT1 and pcDNA3.1-mENT1Δ11 were used as templates for PCR with primers containing the appropriate restriction enzyme cut sites (5′HindIII-mENT1 and 3′mENT1-Kpn1; Table 1) for ligation into the p3×FLAG-CMV10 vector. PCR products were separated on 1.2% agarose gels containing ethidium bromide, cut with the appropriate restriction enzyme, and ligated into p3×FLAG-CMV10. DH5$\alpha$ subcloning efficiency *E. coli* cells were transformed with the plasmid constructs using 42°C heat shock according to manufacturer's protocol (Invitrogen) and plated on Luria-Bertani broth-agar plates containing 100 $\mu$g/ml ampicillin. Plasmid DNA was isolated from transformed DH5$\alpha$ cells according to manufacturer's protocols (QIAGEN).

**Stable Transfections.** PK15-NTD cells were transfected with pcDNA3.1-mENT1, pcDNA3.1-mENT1Δ11, p3×FLAG-CMV10-mENT1, or p3×FLAG-CMV10-mENT1Δ11 using Lipofectamine 2000. The ratio of DNA to Lipofectamine 2000 was 1:3, using approximately 4.0 $\mu$g of plasmid DNA. Transfected cells were selected based on survival in 500 $\mu$g/ml G418, and individual cell colonies were isolated after limiting dilution of the surviving cells. The PK15-mENT1 and PK15-mENT1Δ11 cell lines were maintained at 37°C in a 5% $CO_2$ humidified atmosphere in vented tissue culture flasks containing modified Eagle's medium supplemented with 10% (v/v) bovine growth serum (BGS), 100 units of penicillin, 100 $\mu$g/ml of streptomycin, 0.1 mM nonessential amino acids, 1 mM sodium pyruvate, and 300 $\mu$g/ml G418. mRNA was collected from each cell clone and tested for the presence of the respective mENT1 or mENT1Δ11 transcript by RT-PCR using primers spanning the open reading frame of mENT1 (Table 1).

**Immunoblotting of Transiently Transfected U2-OS Cells.** Transient transfection of U2-OS cells with p3×FLAG-mENT1 and p3×FLAG-mENT1Δ11 was conducted to confirm that the encoded proteins were being properly expressed. U2-OS cells were grown in Dulbecco's modified Eagle's medium with 10% BGS (v/v), 100 units of penicillin and 100 $\mu$g/ml streptomycin. p3×FLAG-mENT1, p3×FLAG-mENT1Δ11, or empty p3×FLAG-vector (25 $\mu$g/175-cm$^2$ flask) was diluted in 10 mM Tris-HCl and 1 mM EDTA, pH 7.3, containing 0.25 mM $CaCl_2$. This DNA+$CaCl_2$ solution was then added drop wise to bubbling 2× concentrated HEPES-buffered saline (280 mM NaCl, 50 mM HEPES, and 1.5 mM $Na_2HPO_4$, pH 7.05). The mixture was incubated at room temperature for 20 min to form a calcium precipitate and was then added to 40% confluent U2-OS cells in a 175-cm$^2$ flask. The cells were incubated with the precipitate overnight (~16 h) at 37°C in a 5% $CO_2$ atmosphere, then washed with PBS and fresh media was added. Cells were harvested 48 h after initial transfection for the preparation of cell membranes.

TABLE 1

PCR primer sequences

The restriction enzyme recognition sequence is underlined. Primer names beginning with 5′ are forward primers, and those beginning with 3′ are reverse primers.

| Primer Name | Sequence (5′ to 3′) |
|---|---|
| 5′mENT1 | GCA AGA GCC AGA GGG AGG GAG |
| 3′mENT1-Kpn1 | CTT GTT AAG GGC ACT TGT GTG AGG TAC CCG GC |
| 5′HindIII-mENT1 | GGC CAA GCT TAT GAC AAC CAG T |
| 5′hENT1 | GGG AAC TAG TAG AAC ACC ATC ACC ATG ACA AC |
| 3′hENT1 | TCC TTC CTG TTC CGG GCA ATT GTA TCG ATA A |

U2-OS cells expressing p3×FLAG-mENT1, p3×FLAG-mENT1Δ11, or empty vector were removed from their flasks with 0.05% Trypsin/EDTA and resuspended in 5 mM sodium phosphate buffer (5 mM $Na_2HPO_4$, pH 7.2) containing a mammalian protease inhibitor cocktail. Cells were incubated in the lysis buffer for 30 min on ice and were subjected to sonication using a Sonic Dismembrator model 150 (Thermo Fisher Scientific, Waltham, MA) (setting 5, 30 s × 3). Cell/membrane suspensions were then centrifuged (4°C, 3000*g* × 30 min) to pellet nuclei and unbroken cells. The supernatant was centrifuged (4°C) for 1 h at 30,000*g*, and the pelleted membranes were suspended in 5 mM sodium phosphate lysis buffer containing protease inhibitor cocktail. Bradford colormetric protein assays (Thermo Fisher Scientific, Waltham, MA) were performed on each membrane preparation to quantify total protein yield.

For immunoblotting, 20 $\mu$g of membrane protein was denatured for 2 min at 100°C in SDS sample buffer (0.5M Tris-Cl, pH 6.8, 30% glycerol, 10% SDS, 0.6 M dithiothreitol, and 0.0012% bromphenol blue) and subjected to SDS-polyacrylamide gel electrophoresis on a 12% acrylamide gel. Samples were then transferred to polyvinylidene difluoride (PVDF) membranes using a Trans-Blot SD Semi-Dry Transfer Cell (Bio-Rad Laboratories, Hercules, CA). The PVDF membranes were blocked overnight with 5% skim milk in TBS-T buffer (0.5 mM Tris, 13.8 mM NaCl, 2.7 mM KCl, and 0.01% Tween 20). After 3 washes of 10 min each in fresh TBS-T buffer, PVDF membranes were incubated with primary polyclonal rabbit anti-FLAG antibody for 2 h at room temperature (1:1000 dilution, 3% skim milk in TBS-T buffer). After three washes of 10 min each with TBS-T buffer, PVDF membranes were incubated with polyclonal goat anti-rabbit secondary antibody conjugated to horseradish peroxidase (1:5000 dilution, 3% skim milk in TBS-T buffer) for 1 h at room temperature. Antigen reactivity was detected using LumiGLO Chemiluminescent Substrate (Millipore Bioscience Research Reagents, Temecula, CA). Molecular mass was determined by comparing $R_f$ values against a Benchmark Prestained Protein Ladder.

**[$^3$H]NBMPR Binding.** Cells were removed from flasks by trypsinization [0.05% (v/v) trypsin and 0.53 mM EDTA, 5 min, 37°C] and diluted with their respective media containing 10% (v/v) BGS and collected by centrifugation. Cell pellets were washed once by resuspension/centrifugation in isotonic *N*-methyl-glucamine (NMG) buffer, pH 7.25, containing 140 mM NMG, 5 mM KCl, 4.2 mM $KHCO_3$, 0.36 mM $K_2HPO_4$, 0.44 mM $KH_2PO_4$, 10 mM HEPES (sodium free), 0.5 mM $MgCl_2$, and 1.3 mM $CaCl_2$ and then resuspended in this buffer for subsequent assays. Cell concentrations were determined routinely using a hemocytometer. In some cases, cells were incubated for 30 min on ice with 300 $\mu$M NEM, and then washed four times with NMG buffer to remove unreacted NEM before use in the binding assays.

PK15-NTD, PK15-mENT1, or PK15-mENT1Δ11 (± 3×FLAG) cells, and isolated membranes prepared as described above, were incubated with [$^3$H]NBMPR using procedures that we have described previously (Bone et al., 2007). Nonspecific binding of [$^3$H]-NBMPR was defined as that seen in the presence of 10 $\mu$M NBTGR. This concentration of NBTGR is 1000-fold greater than its $K_I$ for inhibition of [$^3$H]NBMPR binding to ENT1 (Hammond, 1991). Specific binding of [$^3$H]NBMPR was calculated as total minus nonspecific binding. Nonlinear regression analysis (Prism ver. 4.0; GraphPad Software, San Diego, CA) was used to fit rectangular hyperbolic curves to the site-specific binding of [$^3$H]NBMPR plotted against the free [$^3$H]NBMPR concentration at steady-state.

**[$^3$H]NBMPR Photoaffinity Labeling.** Membranes prepared from PK15-mENT1 and PK15–mENT1Δ11 cells were photolabeled with [$^3$H]NBMPR as we have described previously (Hammond and

Johnstone, 1989). In brief, membranes were incubated with 5 nM [$^3$H]NBMPR for 40 min at room temperature to allow for steady-state binding. Dithiothreitol (10 mM final conc.) was then added and the mixture was placed in a Petri dish on ice and exposed to 45 s of UV light (repeated 3 times with 1 min cooling on ice between UV exposures) from a 200-W mercury-arc lamp at a distance of 4 cm, with constant stirring with a magnetic stir bar. Membranes were washed three times in 5 mM sodium phosphate buffer by centrifugation at 10,000*g* for 3 min, and suspended in Laemmli's SDS-PAGE buffer and incubated at 50°C for 5 min to denature protein. Solubilized membranes were electrophoresed on a 6% SDS-polyacrylamide stacking gel and 5 to 15% gradient SDS-polyacrylamide separating gel. Gels were then fixed in 5% acetic acid, and each gel lane was cut into 2-mm slices for analysis of [$^3$H]content. Radioactivity was plotted against the distance traveled (mm) in the gel and was compared with the reference protein ladder to determine approximate molecular mass of the radiolabeled proteins.

**[$^3$H]Substrate Uptake.** To compare the kinetic properties of substrate translocation by mENT1Δ11 and mENT1, [$^3$H]2-chloroadenosine and [$^3$H]uridine uptake was examined using methods described previous by our laboratory (Stolk et al., 2005; Bone et al., 2007). In brief, cells were incubated with [$^3$H]substrate (± test inhibitors) in 1.5-ml microcentrifuge tubes over a 200-μl layer of 84% silicone/16% light mineral oil. Uptake reactions were terminated by centrifugation of the cells through the oil layer followed by digestion of the cell pellet in 1 M NaOH. Transporter-mediated uptake was defined as the total cell accumulation of radiolabel minus the amount of cell associated radiolabel in the presence of a supramaximal inhibitory concentration (10 μM) of the ENT inhibitors NBTGR and dipyridamole. In some cases, cells were incubated with 300 μM NEM

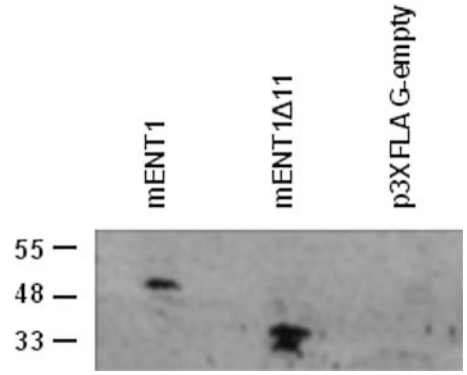


**Fig. 2.** Western blots of mENT1 and mENT1Δ11. U2-OS cells were transiently transfected with either 3×FLAG-mENT1, 3×FLAG-mENT1Δ11, or the empty 3×FLAG-CMV10 vector, and membranes prepared from these cells were electrophoresed on 12% SDS-polyacrylamide gels and transferred to PVDF membranes. The blots were incubated with primary polyclonal rabbit anti-FLAG (1:1000) antibody for 2 h, followed by polyclonal goat anti-rabbit antibody conjugated to horseradish peroxidase (1:5000) for 1 h. The data shown are representative of two independent experiments.

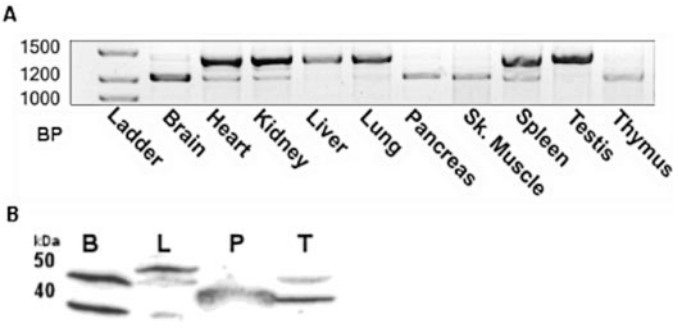


**Fig. 3.** Tissue distribution of mENT1 and mENT1Δ11. A, RT-PCR of ENT1 and ENT1Δ11 from the indicated mouse tissues was performed using oligonucleotide primers spanning the coding region of mENT1. The mENT1Δ11 transcript (lower band) is 1250 bp in size compared with the 1500-bp full-length mENT1 (upper band) on 2.0% agarose gels stained with ethidium bromide. Data shown are representative of three independent RT-PCR reactions using tissues from different mice. B, immunoblots obtained using anti-mENT1antibody in brain (B), liver (L), pancreas (P), and testis (T) tissue homogenates. The predicted sizes of mENT1 and mENT1Δ11 are 50 and 40 kDa, respectively.

TABLE 2

Comparison of the functional characteristics of mENT1 and mENT1Δ11

Each value is the mean ± S.E.M. from at least four independent experiments.

| | mENT1 | mENT1Δ11 |
|---|---|---|
| [$^3$H]NBMPR binding | | |
| $K_d$ (nM) | 0.19 ± 0.02 | 0.14 ± 0.02 |
| $B_{max}$ (sites/cell × $10^3$) | 592 ± 16 | 600 ± 21 |
| [$^3$H]2-Chloroadenosine uptake | | |
| $K_m$ (μM) | 43 ± 12 | 66 ± 22 |
| $V_{max}$ (pmol/μl/s) | 4.4 ± 1.7 | 3.5 ± 1.1 |
| Inhibitor affinity ($K_i$) | | |
| NBMPR (nM) | 0.45 ± 0.16 | 0.94 ± 0.47 |
| Dipyridamole (nM) | 17 ± 8 | 9 ± 3 |
| Dilazep (nM) | 7.2 ± 2.0 | 14 ± 8 |
| Draflazine (nM) | 0.8 ± 0.3 | 1.0 ± 0.5 |
| Adenosine (μM) | 4.7 ± 2.0 | 2.6 ± 1.1 |
| Uridine (μM) | 213 ± 45 | 165 ± 71 |

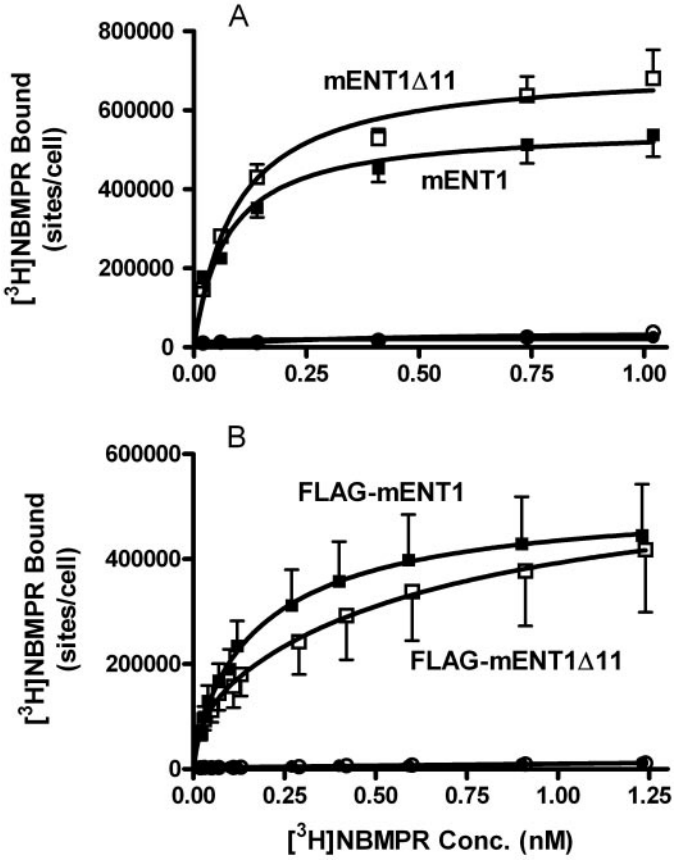


**Fig. 4.** Binding of [$^3$H]NBMPR to PK15 cells transfected with mENT1 or mENT1Δ11 without (A) and with (B) a FLAG-epitope tag on the N terminus. Cells expressing mENT1 (closed symbols) or mENTΔ11 (open symbols) were incubated with a range of concentrations of [$^3$H]NBMPR (abscissa) in the presence (nonspecific binding, circles) and absence (total binding, squares) of 10 μM NBTGR. Each point represents the mean ± S.E.M. of the number of NBMPR binding sites per cell (ordinate) from five independent experiments conducted in duplicate.

for 30 min on ice and then washed extensively with NMG buffer (4 times) before assessment of [$^3$H]2-chloroadenosine uptake.

**Tissue Distribution of mENT1 and mENT1Δ11.** To examine the relative endogenous distribution of mRNA transcript and protein corresponding to mENT1 and mENT1Δ11, a range of tissues (heart, lungs, liver, kidney, brain, pancreas, thymus, skeletal muscle, spleen, and testes) from three male C57BL/6 mice were isolated and either digested in guanidinium isothiocyanate buffer (4.2 M, containing 25 mM sodium citrate, 1 mM EDTA, and 0.007% β-mercaptoethanol, pH 7.0) for RNA extraction, or snap-frozen in liquid nitrogen for subsequent immunoblotting. Total RNA was isolated using standard phenol-chloroform extraction methods, and mRNA was purified from total RNA using the Sigma mRNA purification kit. cDNA was generated from isolated mRNA, then target transcripts were amplified using Platinum Taq polymerase and primers spanning the full coding region of mENT1 (5′mENT1 and 3′mENT1-Kpn1; Table 1). The 3′ primer is designed to anneal to a region located near the end of exon 12, which is present in both the mENT1 and mENT1Δ11, allowing amplification of both transcripts within a single reaction. PCR products were then electrophoresed on a 2% agarose gel with ethidium bromide for approximately 1 h (100 mV, room temperature). Gels were photographed on a digital Alpha Innotech (San Leandro, CA) imaging system.

For immunoblotting, frozen tissue was homogenized in 3 ml/g radioimmunoprecipitation assay buffer containing a protease inhibitor cocktail. Protein samples (100 μg) were denatured for 2 min at 100°C in SDS sample buffer and subjected to SDS-polyacrylamide gel electrophoresis on a 12.5% gel. Samples were then transferred to PVDF membranes, blocked with 5% skim milk in TBS-T for 2 h at room temperature, then immunolabeled with goat anti-ENT1 polyclonal antibody diluted 1:200 in blocking solution at 4°C overnight (~16 h). Membranes were washed in TBS-T and subsequently incubated with donkey anti-goat secondary antibody conjugated to horseradish peroxidase (1:2000 dilution) for 2 h at room temperature. After an additional wash, immunoreactivity was detected using LumiGLO Chemiluminescent Substrate. Molecular mass was determined by comparing $R_f$ values against a Benchmark Prestained Protein Ladder. Specificity of the ENT1 antibody was confirmed by its lack of immunoreactivity to membranes prepared from PK15NTD cells that do not express ENT1.

To investigate the existence of a human ENT1 splice variant analogous to mENT1Δ11, human major tissue cDNA I and II (Biochain Institute, Hayward, CA) isolated from brain, heart, kidney, liver, lung, pancreas, placenta, spleen, and skeletal muscle were screened by PCR, using the conditions described above, with primers designed to span the open reading frame of hENT1 (5′hENT1 and 3′hENT1;Table 1). mRNA was also isolated from human umbilical microvascular endothelial cells and human U2-OS cells and screened for ENT1Δ11 like transcripts as described above.

**Statistical and Data Analyses.** All data were analyzed using Lotus 1–2-3 1997 and [$^3$H]NBMPR and [$^3$H]substrate uptake data were fit to both a one- and two-site model (Prism 4.0, GraphPad Software) and each curve was analyzed for accuracy of fit to the data set by the $F$ test ($P < 0.05$). Data are represented as mean ± S.E.M. from replicate independent experiments conducted in duplicate. Differences were assessed by paired or unpaired Student's $t$ test, as appropriate, with $P < 0.05$ considered significant.

## Results

**mENT1Δ11 Structure.** The predicted membrane topology of mENT1Δ11 is shown in Fig. 1. The amino acid sequence corresponds to the variant of mENT1 with an arginine at position 254 (mENT1a; Genbank accession no. AF131212.1). Examination of the mENT1 gene indicates that mENT1Δ11 arises from the splicing of the 3′ end of exon 10 to the 5′ splice site of exon 12. This results in a frame-shift at the splice point leading to a premature stop codon after the translation of five unique C-terminal amino acids (tryptophan, glutamate, glutamine, threonine, and serine). mENT1Δ11 is predicted to have nine TM domains and cytoplasmic C and N termini.

To confirm that ENT1Δ11 did indeed encode a truncated protein. Membranes prepared from U2-OS cells transiently transfected with either p3×FLAG-mENT1, p3×FLAG-mENT1Δ11, or the empty p3×FLAG-vector were subjected to electrophoresis and immunoblotting with polyclonal rabbit anti-FLAG antibody. Bands corresponding to the predicted 33-kDa p3×FLAG-mENT1Δ11 and the 48 kDa p3×FLAG-mENT1 were detected, indicating that these proteins were expressed and were of the expected size (Fig. 2).

**Tissue Distribution.** RT-PCR was performed using cDNA prepared from mRNA isolated from several mouse tissues. mENT1Δ11 transcript was detected as a ~1250-bp band compared with full-length mENT1 (~1500 bp) on 2% agarose gels stained with ethidium bromide. These studies showed that mENT1Δ11 expression is ubiquitous, similar to the distribution of mENT1, appearing in brain, heart, kidney, liver, lung, pancreas, skeletal muscle, spleen, thymus, and testes. However, there were distinct differences in the relative ratio of mENT1 to mENT1Δ11 in some tissues (Fig. 3). Tissues with a higher relative ratio of mENT1Δ11 to mENT1 included thymus, brain,

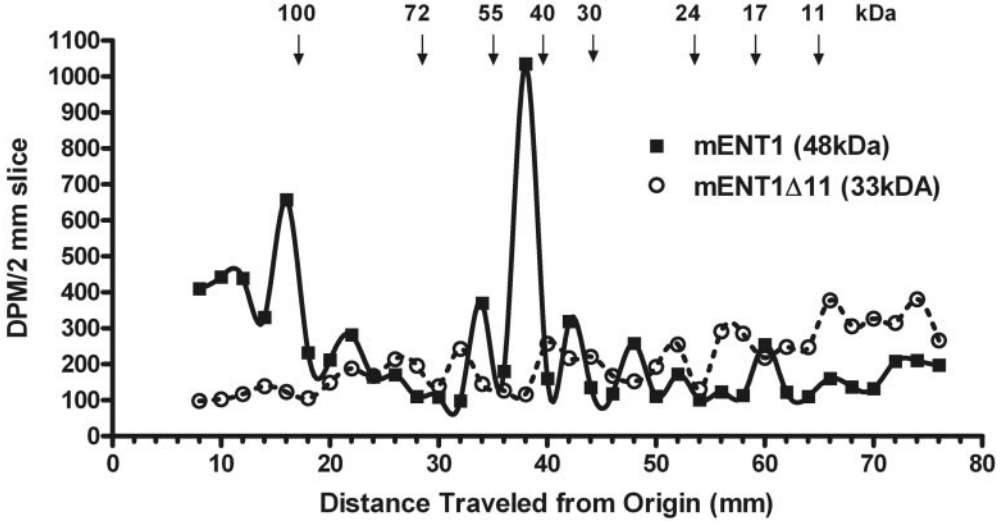


**Fig. 5.** Photoaffinity labeling of PK15-mENT1 and PK15-mENT1Δ11 membrane proteins with [$^3$H]NBMPR. PK15-mENT1 and PK15-mENT1Δ11 cell membranes were incubated, in parallel, with 50 nM [$^3$H]NBMPR for 1 h on ice and then exposed to UV light (~365 nm) and separated on SDS-PAGE gels as described in the text. The amount of radioactivity associated with each 2 mm gel slice (dpm) are plotted against the gel migration distance and compared with a set of protein standards as shown at the top of the figure. Data shown are representative of five independent experiments.

skeletal muscle and pancreas. The 1250-bp bands from skeletal muscle and brain were extracted and sequenced to confirm their identity as mENT1Δ11.

Examination of a number of human tissues and cell-lines by RT-PCR revealed a hENT1 PCR product of approximately 1500 base pairs in all tissues and cells tested. There was no evidence of a smaller PCR product analogous to mENT1Δ11 in any of the human tissues examined (data not shown).

To confirm that the mENT1Δ11 protein was actually being expressed in mouse tissues, mENT1 antibody reactivity was assessed in mouse brain, testis, liver, and pancreas. Brain and testis immunoblots had bands at ~45 to 50 kDa and ~35 to 40 kDa, which correspond to the expected sizes of the full-length mENT1 and mENT1Δ11, respectively. However, liver had predominantly the 50-kDa mENT1, and pancreas showed predominantly the 40-kDa mENT1Δ11. The double band in liver at the 50-kDa range probably represents multiple glycosylation states of mENT1 (Vickers et al., 1999).

**[$^3$H]NBMPR Binding.** PK15-mENT1 and PK15–mENT1Δ11 cells bound [$^3$H]NBMPR with similar affinity ($K_d$ < 0.2 nM) to more than 500,000 sites per cell (Table 2; Fig. 4A). The PK15–3×FLAG-mENT1 cells also bound [$^3$H]-NBMPR to a single class of site with a $K_d$ of 0.15 ± 0.01 to a maximum of 52 ± 11 × $10^4$ sites per cell (Fig. 4B). However, [$^3$H]NBMPR binding to the PK15–3×FLAG-mENT1Δ11 cells fit best (2 independent cell clones tested) to a two site model with 55 ± 15 × $10^4$ sites/cell having an affinity of 1.9 ± 0.8 nM, and an additional 13.5 ± 4 × $10^4$ sites/cell having an affinity of 0.021 ± 0.005 nM (Fig. 4B; Table 2). The untransfected PK15-NTD cell line showed no apparent specific binding of [$^3$H]NBMPR (data not shown).

Photolabeling of PK15-mENT1 cell membranes with [$^3$H]-NBMPR led to a distinct radiolabeled band on SDS-PAGE gels in the 48-kDa range, which is the expected size of the mENT1 protein (Fig. 5). There was also an additional peak seen at approximately 100 kDa, possibly representing mENT1 dimers. PK15-mENT1Δ11 cell membranes were treated with [$^3$H]NBMPR and exposed to UV light in parallel with the PK15-mENT1 membranes. The expected size of mENT1Δ11 protein was 33 kDa; however, no distinct radiolabeled peaks were observed on gels of the PK15-mENT1Δ11 proteins after exposure to [$^3$H]NBMPR (Fig. 5), even though these same isolated membranes bound [$^3$H]NBMPR with high affinity in reversible binding assays (data not shown).

**[$^3$H]Substrate Uptake.** PK15-mENT1Δ11 cells accumulated 10 μM [$^3$H]2-chloroadenosine (a purine substrate for ENT1) with an initial rate of transporter-mediated uptake of 0.49 ± 0.10 pmol/μl/s, to a maximum intracellular concentration of 23 ± 3 μM (Fig. 6A). This rate of uptake was similar to that discerned previously for mENT1a-transfected PK15 cells (Bone et al., 2007). To determine whether there was a change in permeant selectivity in the mENT1Δ11 variant, the uptake of the pyrimidine substrate uridine was also examined. PK15-mENT1 and PK15-mENT1Δ11 cells accumulated 100 μM [$^3$H]uridine in a transporter-dependent manner with initial rates of 2.1 ± 0.3 and 4.4 ± 0.7 pmol/μl/s, respectively (Fig. 6B). Based on these initial time course studies, an incubation time of 15 sec was selected for the assessment of the rate of uptake of a range of concentrations of [$^3$H]2-chloroadenosine. PK15-mENT1Δ11 cells transported 2-chloroadenosine with affinity ($K_m$ = 66 μM) similar to that of the PK15-mENT1 cells ($K_m$ = 43 μM). Likewise, there was no significant difference in the $V_{max}$ of [$^3$H]2-chloroadenosine transport in the two cell lines (3.5 ± 1.1 and 4.4 ± 1.7pmol/μl/s for the PK15-mENT1Δ11 and PK15-mENT1a cells, respectively). (Fig. 6C). Similar studies using a 5-s incubation period conducted with the PK15–3×FLAG-

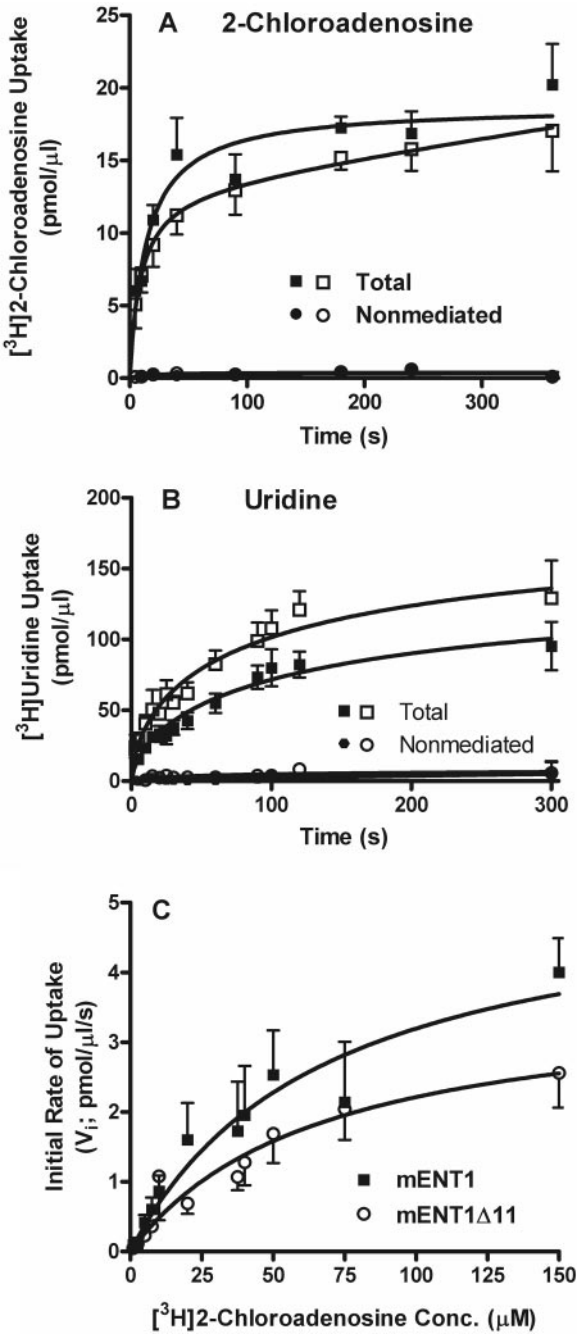


**Fig. 6.** [$^3$H]2-Chloroadenosine and [$^3$H]uridine uptake by PK15-mENT1 (closed symbols) and PK15-mENT1Δ11 (open symbols) cells. Cells were incubated with 10 μM [$^3$H]2-chloroadenosine (A) or 100 μM [$^3$H]uridine (B) for the times indicated (abscissa) in the presence (nonmediated uptake; circles) or absence (total uptake; squares) of 8 μM dipyridamole/NBTGR. Each point represents the mean ± S.E.M. of the cellular accumulation of [$^3$H]substrate (picomoles per microliter of total cell water) at each time point from at least five independent experiments conducted in duplicate. C, initial rate of transporter-mediated (total − nonmediated) uptake of a range of concentrations of [$^3$H]2-chloroadenosine in both the PK15-mENT1 and PK15-mENT1Δ11 cells. Each point represents the mean ± S.E.M. from five independent experiments.

mENT1 and PK15–3×FLAG-mENT1Δ11 cells revealed $K_m$ values of 44 ± 18 and 43 ± 11 μM, respectively, and $V_{max}$ values of 17 ± 4 and 19 ± 3 pmol/μl/s, respectively.

Several known ENT1 inhibitors (NBMPR, dilazep, draflazine, and dipyridamole) and endogenous substrates (adenosine and uridine) were assessed for their abilities to block [$^3$H]2-chloroadenosine uptake by PK15-mENT1 and PK15-mENT1Δ11 cells (Fig. 7). The pseudo-Hill coefficients for all inhibitors were not significantly different from −1; therefore, the Cheng-Prusoff equation (Cheng and Prusoff, 1973) was used to calculate $K_I$ values. NBMPR was the most effective inhibitor with $K_I$ values of 0.5 ± 0.2 and 0.9 ± 0.3 nM for PK15-mENT1 and PK15–mENT1Δ11, respectively, followed by draflazine, dilazep, and dipyridamole. Adenosine was approximately 50 times more effective at inhibiting [$^3$H]2-chloroadenosine uptake than was uridine in both the PK15-mENT1 (4 ± 2 and 200 ± 29 μM, respectively) and the PK15-mENT1Δ11 (3 ± 1 and 165 ± 71 μM, respectively). There were no significant differences in $K_I$ values (Student's paired $t$ test, $P < 0.05$) for PK15-mENT1Δ11 compared with PK15-mENT1 for any of the inhibitors or substrates tested (Table 2).

**Effect of NEM.** Treatment of PK15–3×FLAG-mENT1 with 300 μM NEM for 30 min on ice increased both the $K_d$ and $B_{max}$ of [$^3$H]NBMPR binding to 3×FLAG-mENT1 compared with untreated control cells. In contrast, NEM affected only the higher affinity component of the biphasic [$^3$H]NBMPR binding to the PK15–3×FLAG-mENT1Δ11 cells. NEM also increased both the $K_m$ and $V_{max}$ of [$^3$H]2-chloroadenosine uptake by the full-length mENT1 but had no significant effect on the mENT1Δ11 variant (Fig. 8, Table 3). Similar uptake data (±NEM) were obtained using PK15-NTD cells transfected with either the 3×FLAG-tagged or non–FLAG-tagged versions of mENT1 and mENT1Δ11 (data not shown).

## Discussion

The data presented in this report indicate that the last three transmembrane domains of mENT1 are not required for membrane expression, translocation activity or ligand binding of mENT1. No differences were noted between the full-length mENT1 and the truncated mENT1Δ11 in terms of substrate or inhibitor affinity. mENT1 and mENT1Δ11 are both widely expressed but differ in their relative levels of expression in a number of tissues, suggesting that the expression of the truncated variant is regulated differently than that of the full-length ENT1. Of the tissues examined, brain, thymus, skeletal muscle, and pancreas have more mENT1Δ11 transcript compared with the full-length mENT1. In contrast, liver shows mostly the full-length mENT1 transcript. A compatible profile of mENT1 immunoreactivity was also seen in these tissues; brain and testis had both a ~45- to 50-kDa band and a 35- to 40-kDa band, but liver showed only the 45- to 50-kDa band, and pancreas only the 35- to 40-kDa variant. The fact that the mRNA profile does not exactly match the protein ratio of mENT1:

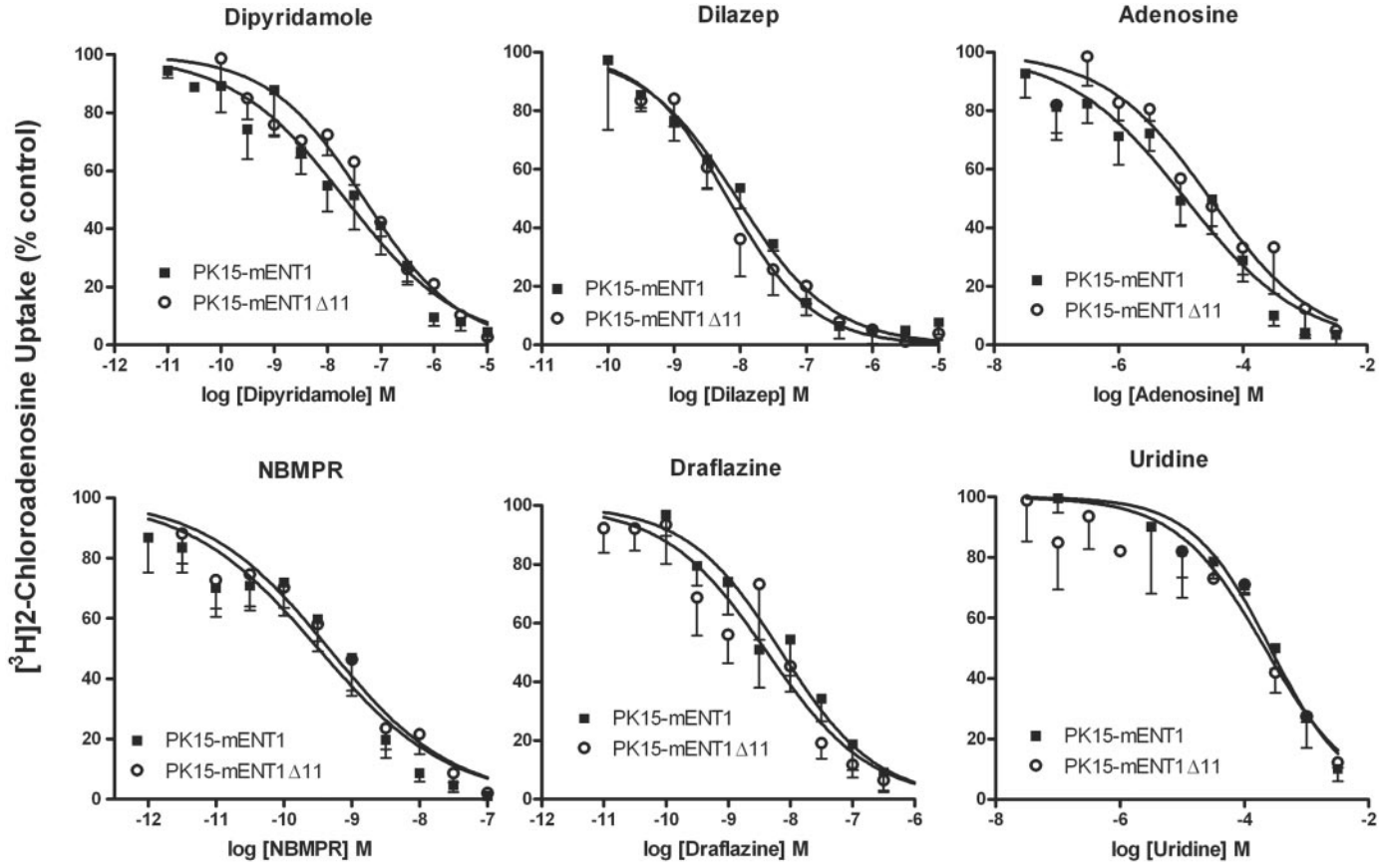


**Fig. 7.** Inhibition of [$^3$H]2-chloroadenosine uptake by inhibitors and substrates of mENT1. PK15-mENT1 (■) and PK15-mENT1Δ11 (○) cells were incubated with 10 μM [$^3$H]2-chloroadenosine for 15 s in the presence and absence of the indicated concentrations of test agents. Each point represents the mean ± S.E.M. from at least four independent experiments conducted in duplicate.

mENT1Δ11 in some tissues (e.g., testis) may be due to differences in mRNA translation rates or stability of the two transcripts or may reflect an age related difference in the expression of the mENT1 variants (the Western blots and PCR experiments were done on tissues from different animals). The slight differences in size of the mENT1 bands between tissues are probably due to differences in the extent of glycosylation. In general, these molecular masses are a bit lower than the predicted sizes of mENT1 (50 kDa) and mENT1Δ11 (40 kDa) but are similar to those noted in other studies for photoaffinity-labeled mENT1 (Hammond and Johnstone, 1989). The tissues with high levels of mENT1Δ11 all tend to be highly metabolically active tissues, and thus one could speculate that the mENT1Δ11 variant may be expressed in response to an enhanced requirement for nucleoside salvage to support the increased metabolic activity. Unfortunately, there is insufficient functional data available in the literature at this time to confirm that these tissues actually do have enhanced nucleoside transport capacity; most studies on nucleoside transport are conducted in isolated cell lines.

The only functional differences noted between mENT1 and mENT1Δ11 were that 1) mENT1Δ11 cannot bind [$^3$H]NBMPR irreversibly upon exposure to UV light and 2) [$^3$H]2-chloroadenosine uptake by mENT1Δ11 is insensitive to the sulfhydryl reagent NEM. The inability of [$^3$H]NBMPR to photolabel mENT1Δ11 suggests that the loss of this C-terminal region of mENT1 removes the residue that NBMPR normally cross-links to or that a critical residue has shifted

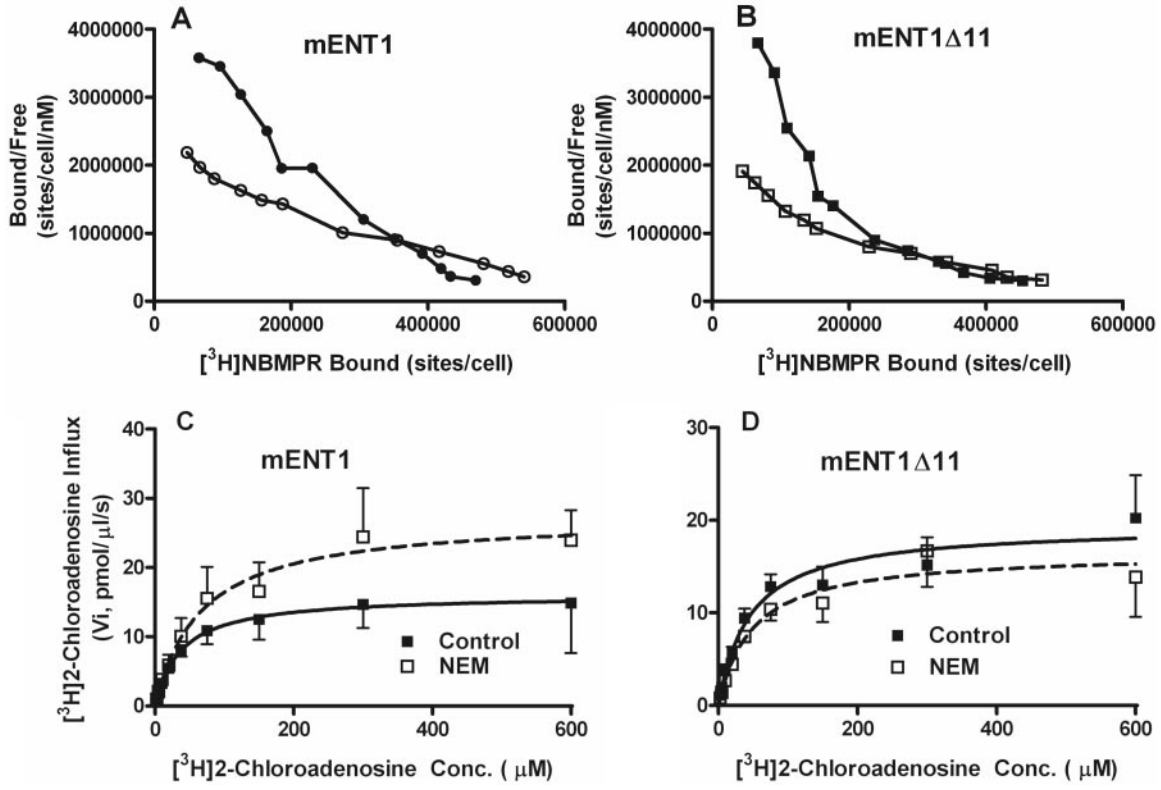


**Fig. 8.** Effect of NEM on [$^3$H]NBMPR binding (top) and [$^3$H]2-chloroadenosine uptake (bottom) in PK15 cells transfected with either 3×FLAG-mENT1 (left) or 3×FLAG-mENT1Δ11 (right panels). A and B, cells with (○) and without (●) pretreatment with 300 μM NEM were incubated with a range of concentrations of [$^3$H]NBMPR in the presence and absence of 10 μM NBTGR to determine the amount of specific binding to ENT1. Results are represented as Scatchard plots (bound versus bound/free), each point being the mean of five independent experiments. C and D, cells, with (□) and without (■) pretreatment with 300 μM NEM, were incubated with a range of concentrations of [$^3$H]2-chloroadenosine in the presence and absence of 10 μM dipyridamole/NBMPR to determine the amount of transporter-mediated uptake of [$^3$H]2-chloroadenosine. Each point represents the mean ± S.E.M. of the initial rate of [$^3$H]2-chloroadenosine uptake at each concentration from five independent experiments conducted in duplicate.

TABLE 3

Effect of NEM on NBMPR binding and 2-chloroadenosine uptake by PK15 cells transfected with mENT1 or mENT1Δ11

Each value is the mean ± S.E.M. from at least four independent experiments.

| | mENT1 | | mENT1Δ11 | |
|---|---|---|---|---|
| | Control | NEM | Control | NEM |
| NBMPR binding | | | | |
| $K_d$1 (nM) | 0.15 ± 0.01 | 0.53 ± 0.15* | 0.021 ± 0.005 | 0.025 ± 0.008 |
| $K_d$2 (nM) | | | 1.9 ± 0.9 | 0.61 ± 0.07* |
| $B_{max}$1 (sites/cell × $10^3$) | 517 ± 111 | 725 ± 128* | 134 ± 40 | 55 ± 20* |
| $B_{max}$2 (sites/cell × $10^3$) | | | 546 ± 146 | 602 ± 133 |
| 2-Chloroadenosine uptake | | | | |
| $K_m$ (μM) | 44 ± 19 | 95 ± 34* | 43 ± 11 | 55 ± 16 |
| $V_{max}$ (pmol/μl/s) | 17 ± 4 | 27 ± 4* | 19 ± 3 | 18 ± 4 |

* Significant difference from the respective control (Student's $t$ test for paired samples, $P < 0.05$).

position as a result of the structural rearrangement of the protein that is likely to occur in the truncated variant. Given that mENT1Δ11 retains the ability to bind [$^3$H]NBMPR reversibly with high affinity, and the previous finding that the site of UV light induced covalent attachment of [$^3$H]NBMPR to hENT1 is in the N-terminal half of the protein (Kwong et al., 1993), we would argue that the loss of the last three transmembrane domains of mENT1 leads to a conformation change that prevents covalent attachment of the [$^3$H]NBMPR to elements of its binding pocket in the N-terminal part of the protein. It is generally believed that the *S*-nitrobenzyl group of NBMPR is photoactivated upon exposure to UV light; hence the amino acid residue involved in the photoaffinity labeling is probably proximal to the mENT1 region that binds the *S*-nitrobenzyl moiety of NBMPR (Paterson and Oliver, 1971; Young et al., 1983; Shi et al., 1984; Zhu et al., 2003).

We noted biphasic saturation profiles for [$^3$H]NBMPR binding in some of the models tested in this study. In other cases, although not obviously biphasic, [$^3$H]NBMPR binding had Hill coefficients of less than unity. These results probably reflect two populations of [$^3$H]NBMPR binding proteins in these heterologous expression models, possibly representing those present at the cell surface (high affinity) and others in intracellular compartments (lower affinity). Similar biphasic [$^3$H]NBMPR binding profiles have been described in Ehrlich ascites tumor cells (Vyas et al., 2002), endothelial cells (Hammond and Archer, 2004), and BeWo cells (Boumah et al., 1992).

Treatment of PK15-mENT1 cells with NEM increased the high-affinity binding of NBMPR and enhanced the uptake of 2-chloroadenosine by mENT. In contrast, NEM had no affect on these parameters in the PK15-mENT1Δ11 cells. There are four cysteine residues in theTM9 - C-terminal region of mENT1. These cysteines are clearly not critical for transporter function because their loss from mENT1Δ11 did not affect 2-chloroadenosine or uridine uptake or [$^3$H]NBMPR binding. These results are compatible with a previous study on the effect of NEM on NBMPR binding to mouse Ehrlich ascites tumor cells, where we found that 100 $\mu$M NEM enhanced the ability of the nucleoside substrates uridine, adenosine, and deoxyadenosine to inhibit NBMPR binding (Vyas et al., 2002). Because treatment of the cells with NEM was conducted on ice, the NEM-induced increase in ENT1 activity was probably not due to trafficking of ENT1 protein from intracellular compartments to the plasma membrane. Rather, NEM treatment may be leading to the activation of cryptic transporters that already exist in the plasma membrane. A similar increase in ENT1-mediated nucleoside uptake, in the absence of increased plasma membrane ENT1 protein, was reported recently by Coe et al. (2002) in response to protein kinase C activation. Regardless of mechanism, this enhancement by NEM is lost in the mENT1Δ11 variant, suggesting that one or more of the four cysteines in the C-terminal region of mENT1 are involved in this effect. Thus we propose that the TM9 to C terminus region of the transporter is functionally linked to, but not directly part of, the [$^3$H]NBMPR binding site and substrate translocation mechanism.

Little is known about the tertiary structure of ENT1. A number of studies have implicated the TMs 3–6 region in the binding of NBMPR and the translocation of substrates (Baldwin et al., 2004). Regions outside of TMs 3–6 have also been shown to affect ligand binding to ENTs, but almost all of the studies implicating specific regions/residues in ligand binding and transporter function have focused on amino acids upstream of TM9 (Visser et al., 2005b, 2007). The exceptions are a study showing that Arg404 of the Leishmania donovani nucleoside transporter LdNT1.1 (corresponding to Arg369 in TM9 of hENT1) is important for function and substrate specificity (Valdés et al., 2006) and a study showing that Leu442 in TM11 of hENT1 is important for substrate selectivity (Visser et al., 2005a). These results are difficult to reconcile with fact that mENT1Δ11, which is missing TMs 9–11 transports both the purine nucleoside 2-chloroadenosine and the pyrimidine nucleoside uridine as effectively as the full-length mENT1. It is possible that a more detailed analysis of the substrate specificity of mENT1Δ11 will reveal subtle differences relative to mENT1. It is noteworthy that mutation of Phe334 in TM8 of hENT1 to tyrosine dramatically enhanced the turnover rate (molecules per second) of the ENT1 transporter (Visser et al., 2007), reminiscent of the effect of NEM on 2-chloroadenosine uptake seen in the present study. These results suggest that TM8 is conformationally linked to the substrate translocation mechanism in TMs 4 and 5, and cysteine residues in the region of TMs 9–11 may affect this interaction.

The ability of ENT proteins to function despite a major C-terminal deletion is not unique to the mouse ENT1. An ENT2 splice variant lacking the last four TM domains has been identified in rabbit (rbENT2a) (Wu et al., 2005). rbENT2a was shown to be expressed to the plasma membrane and remained functional, with some slight differences in substrate affinity and inhibitor sensitivities.

In summary, we have shown that truncation of the mENT1 protein in the intracellular loop before TM9 does not affect the expression or function of the transporter upon stable transfection in PK15-NTD cells. The inability of the truncated mENT1Δ11 variant to be covalently labeled with [$^3$H]NBMPR and its reduced sensitivity to the sulfhydryl reagent NEM highlight potential interactions between the TM 9–11 C-terminal end of the protein and the TM 3–6 region implicated in substrate and inhibitor binding. These results provide important guidelines for future mutagenesis studies aimed at elucidating the tertiary structure of the ENT1 protein and the domains involved in inhibitor binding and substrate translocation.

**References**

Baldwin SA, Beal PR, Yao SY, King AE, Cass CE, and Young JD (2004) The equilibrative nucleoside transporter family, SLC29. *Pflugers Arch* **447:**735–743.

Bone DB, Robillard KR, Stolk M, and Hammond JR (2007) Differential regulation of mouse equilibrative nucleoside transporter 1 (MENT1) splice variants by protein kinase CK2. *Mol Membr Biol* **24:**294–303.

Boumah CE, Hogue DL, and Cass CE (1992) Expression of high levels of nitrobenzylthioinosine-sensitive nucleoside transport in cultured human choriocarcinoma (BeWo) cells. *Biochem J* **288:**987–996.

Cheng Y and Prusoff WH (1973) Relationship between the inhibition constant (K1) and the concentration of inhibitor which causes 50 per cent inhibition (I50) of an enzymatic reaction. *Biochem Pharmacol* **22:**3099–3108.

Coe I, Zhang Y, McKenzie T, and Naydenova Z (2002) PKC regulation of the human equilibrative nucleoside transporter, HENT1. *FEBS Lett* **517:**201–205.

Coe IR, Griffiths M, Young JD, Baldwin SA, and Cass CE (1997) Assignment of the human equilibrative nucleoside transporter (HENT1) to 6p21.1-P21.2. *Genomics* **45:**459–460.

Griffiths M, Beaumont N, Yao SYM, Sundaram M, Boumah CE, Davies A, Kwong FYP, Coe I, Cass CE, Young JD, et al. (1997) Cloning of a human nucleoside transporter implicated in the cellular uptake of adenosine and chemotherapeutic drugs. *Nature Med* **3:**89–93.

Hammond JR (1991) Kinetic analysis of ligand binding to the Ehrlich cell nucleoside transporter: pharmacological characterization of allosteric interactions with the [$^3$H]nitrobenzylthioinosine binding site. *Mol Pharmacol* **39:**771–779.

Hammond JR and Archer RG (2004) Interaction of the novel adenosine uptake inhibitor 3-[1-(6,7-diethoxy-2-morpholinoquinazolin-4-yl)piperidin-4-yl]-1,6-dimethyl-2,4 (1*H*,3*H*)-quinazolinedione hydrochloride (KF24345) with the *Es* and *Ei* subtypes of equilibrative nucleoside transporters. *J Pharmacol Exp Ther* **308:** 1083–1093.

Hammond JR and Johnstone RM (1989) Solubilization and reconstitution of a nucleoside-transport system from Ehrlich ascites-tumour cells. *Biochem J* **262:** 109–118.

Handa M, Choi D, Caldeiro RM, Messing RO, Gordon AS, and Diamond II (2001) Cloning of a novel isoform of the mouse NBMPR-sensitive equilibrative nucleoside transporter (ENT1) lacking a putative phosphorylation site. *Gene* **262:**301–307.

Hyde RJ, Cass CE, Young JD, and Baldwin SA (2001) The ENT family of eukaryote nucleoside and nucleobase transporters: recent advances in the investigation of structure/function relationships and the identification of novel isoforms. *Mol Membr Biol* **18:**53–63.

King AE, Ackley MA, Cass CE, Young JD, and Baldwin SA (2006) Nucleoside transporters: from scavengers to novel therapeutic targets. *Trends Pharmacol Sci* **27:**416–425.

Kiss A, Farah K, Kim J, Garriock RJ, Drysdale TA, and Hammond JR (2000) Molecular cloning and functional characterization of inhibitor-sensitive (MENT1) and inhibitor-resistant (MENT2) equilibrative nucleoside transporters from mouse brain. *Biochem J* **352:**363–372.

Kwong FYP, Wu J-S R, Shi MM, Fincham HE, Davies A, Henderson PJF, Baldwin SA, and Young JD (1993) Enzymic cleavage as a probe of the molecular structures of mammalian equilibrative nucleoside transporters. *J Biol Chem* **268:**22127–22134.

Paterson ARP, and Oliver JM (1971) Nucleoside transport. II. Inhibition by P-nitrobenzylthioguanosine and related compounds. *Can J Biochem* **49:**271–274.

Robillard K, Patrianakos V, and Hammond JR (2006) A novel splice variant of the equilibrative nucleoside transporter 1 (ENT1). *Acta Pharmacologica Sinica* **27 (Suppl 1):**391.

Shi MM, Wu J-SR, Lee C-M, and Young JD (1984) Nucleoside transport: photoaffinity labelling of high-affinity nitrobenzylthioinosine binding sites in rat and guinea pig lung. *Biochem Biophys Res Commun* **118:**594–600.

Stolk M, Cooper E, Vilk G, Litchfield DW, and Hammond JR (2005) Subtype-specific regulation of equilibrative nucleoside transporters by protein kinase CK2. *Biochem J* **386:**281–289.

Valdés R, Liu W, Ullman B, and Landfear SM (2006) Comprehensive examination of charged intramembrane residues in a nucleoside transporter. *J Biol Chem* **281:** 22647–22655.

Vickers MF, Mani RS, Sundaram M, Hogue DL, Young JD, Baldwin SA, and Cass CE (1999) Functional production and reconstitution of the human equilibrative nucleoside transporter (HENT1) in *Saccharomyces cerevisiae*. Interaction of inhibitors of nucleoside transport with recombinant Hent1 and a glycosylation-defective derivative (Hent1/N48q). *Biochem J* **339:**21–32.

Visser F, Baldwin SA, Isaac RE, Young JD, and Cass CE (2005a) Identification and mutational analysis of amino acid residues involved in dipyridamole interactions with human and *Caenorhabditis elegans* equilibrative nucleoside transporters. *J Biol Chem* **280:**11025–11034.

Visser F, Sun L, Damaraju V, Tackaberry T, Peng Y, Robins MJ, Baldwin SA, Young JD, and Cass CE (2007) Residues 334 and 338 in transmembrane segment 8 of human equilibrative nucleoside transporter 1 are important determinants of inhibitor sensitivity, protein folding and catalytic turnover. *J Biol Chem* **282:**14148–14157.

Visser F, Zhang J, Raborn RT, Baldwin SA, Young JD, and Cass CE (2005b) Residue 33 of human equilibrative nucleoside transporter 2 is a functionally important component of both the dipyridamole and nucleoside binding sites. *Mol Pharmacol* **67:**1291–1298.

Vyas S, Ahmadi B, and Hammond JR (2002) Complex effects of sulfhydryl reagents on ligand interactions with nucleoside transporters: evidence for multiple populations of ENT1 transporters with differential sensitivities to N-ethylmaleimide. *Arch Biochem Biophys* **403:**92–102.

Wu SK, Ann DK, Kim KJ, and Lee VH (2005) Fine tuning of rabbit equilibrative nucleoside transporter activity by an alternatively spliced variant. *J Drug Target* **13:**521–533.

Yao SY, Ng AM, Muzyka WR, Griffiths M, Cass CE, Baldwin SA, and Young JD (1997) Molecular cloning and functional characterization of nitrobenzylthioinosine (NBMPR)-sensitive (Es) and NBMPR-insensitive (Ei) equilibrative nucleoside transporter proteins (RENT1 and RENT2) from rat tissues. *J Biol Chem* **272:** 28423–28430.

Young JD, Jarvis SM, Robins MJ, and Paterson ARP (1983) Photoaffinity labeling of the human erythrocyte nucleoside transporter by $N^6$-(p-azidobenzyl)adenosine and nitrobenzylthioinosine: evidence that the transporter is a band 4.5 polypeptide. *J Biol Chem* **258:**2202–2208.

Zhang J, Visser F, King KM, Baldwin SA, Young JD, and Cass CE (2007) The role of nucleoside transporters in cancer chemotherapy with nucleoside drugs. *Cancer Metastasis Rev* **26:**85–110.

Zhu Z, Furr J, and Buolamwini JK (2003) Synthesis and flow cytometric evaluation of novel 1,2,3,4-tetrahydroisoquinoline conformationally constrained analogues of nitrobenzylmercaptopurine riboside (NBMPR) designed for probing its conformation when bound to the es nucleoside transporter. *J Med Chem* **46:**831–837.

**Address correspondence to:** Dr. James R Hammond, Dept. of Physiology and Pharmacology, M266 Medical Sciences Building, University of Western Ontario, London, Ontario, N6A 5C1, Canada. E-mail: jhammo@uwo.ca